Synoptic-scale meteorology modulates aerosol and fog characteristics in coastal Namibia

Huihui Wu[1], Chenjie Yu[1], Vincent Michoud[1], Hendrik Andersen[2,3], Aneska Richter[4], Henno Havenga[4], Brigitte Language[4], Daniel Tetteh Quaye[5], Khanneh Wadinga Fomba[5], Laurent Poulain[5], Uwe Käfer[5], Muguette Allegre[1], Cécile Gaimoz[1,a], Mathieu Cazaunau[1], Maxime Feingesicht[1], Hupenyu Allan Mupambwa[6], Stuart John Piketh[4], and Paola Formenti[1]

[1] Université Paris Cité and Univ Paris Est Créteil, CNRS, LISA, F-75013 Paris, France
[2] Karlsruhe Institute of Technology (KIT), Institute of Meteorology and Climate Research Atmospheric Trace Gases and Remote Sensing, Karlsruhe, Germany
[3] Karlsruhe Institute of Technology (KIT), Institute of Photogrammetry and Remote Sensing, Karlsruhe, Germany
[4] School of Geo- and Spatial Science, North-West University, Potchefstroom, South Africa
[5] Leibniz Institute for Tropospheric Research (TROPOS), Leipzig, Germany
[6] Sam Nujoma Marine and Coastal Resources Research Centre, University of Namibia, Sam Nujoma Campus, Private Bag 462, Henties Bay 13005, Namibia
[a] now at: CNRS INSU Division Technique, Gif-Sur-Yvette, France

Correspondence to: Chenjie Yu (chenjie.yu@lisa.ipsl.fr) and Paola Formenti (paola.formenti@lisa.ipsl.fr)

Supplementary

Table S1. Values of hygroscopic parameter kappa (κ) and densities used for chemical components

Species	Density (kg m^{-3})	kappa (κ)
Sulfuric acid, H_2SO_4	1830[a]	0.68[d]
Ammonium sulfate, $(NH_4)_2SO_4$	1769[a]	0.52[d]
Ammonium bisulfate, NH_4HSO_4	1780[a]	0.56[d]
Ammonium nitrate, NH_4NO_3	1720[a]	0.68[d]
Ammonium chloride, NH_4Cl	1527[b]	0.93[d]
Organics, OA	1400[c]	(0.18±0.04) × O:C + 0.03[e]

[a]Topping et al. (2005). [b]Silvergren et al. (2014). [c]Alfarra et al. (2006). [d]Liu et al. (2014). [e]Lambe et al. (2011).

Table S2. Summary of fog events observed during the campaign.

Event ID	Start time	End time	Duration (h)	formation
E1	14/05 06:30	14/05 09:00	2.5	lowering stratus
E2	14/05 23:00	15/05 07:15	8.25	lowering stratus
E3	24/05 02:40	24/05 03:15	0.42	locally
E4	25/05 04:10	25/05 06:10	2.0	locally
E5	26/05 04:06	26/05 07:10	4.07	locally
E6	28/05 09:00	28/05 20:36	10.6	lowering stratus
E7	29/05 02:00	29/05 05:09	2.15	lowering stratus

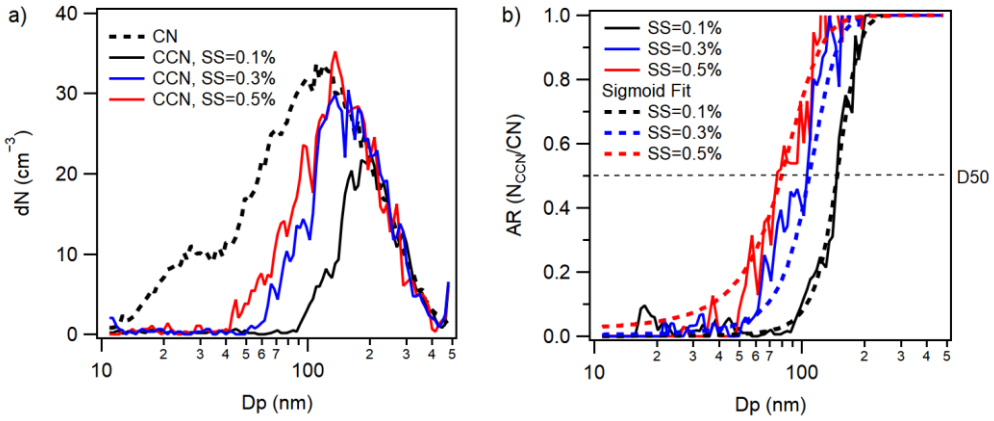


Figure S1. (a) Examples of the size-resolved CN and N_{CCN} measurements. (b) Examples of the size-resolved CCN activation fraction (N_{CCN}/CN), and this curve can be fitted in sigmoid function to derive D_c.

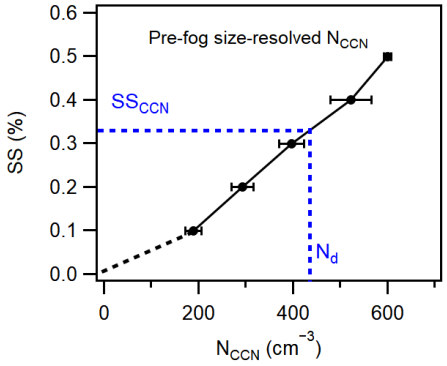


Figure S2. SS_{CCN} is derived from the pre-fog SS-resolved N_{CCN} measurements and N_d. The dashed black line represents linear interpolation from N_{CCN} measurements at two lower SS set points.

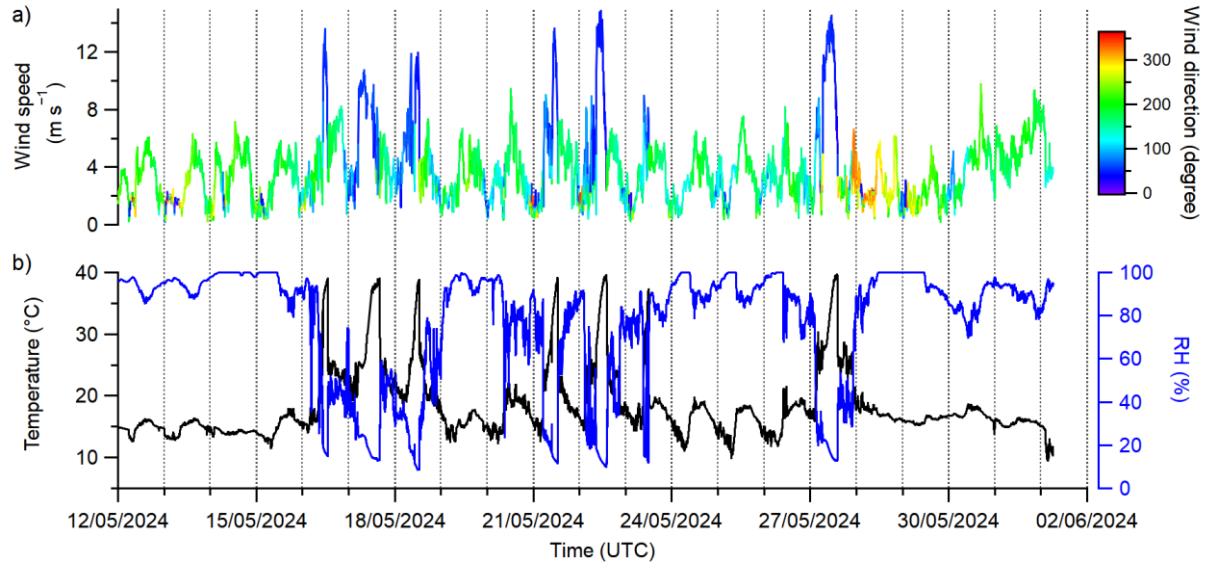
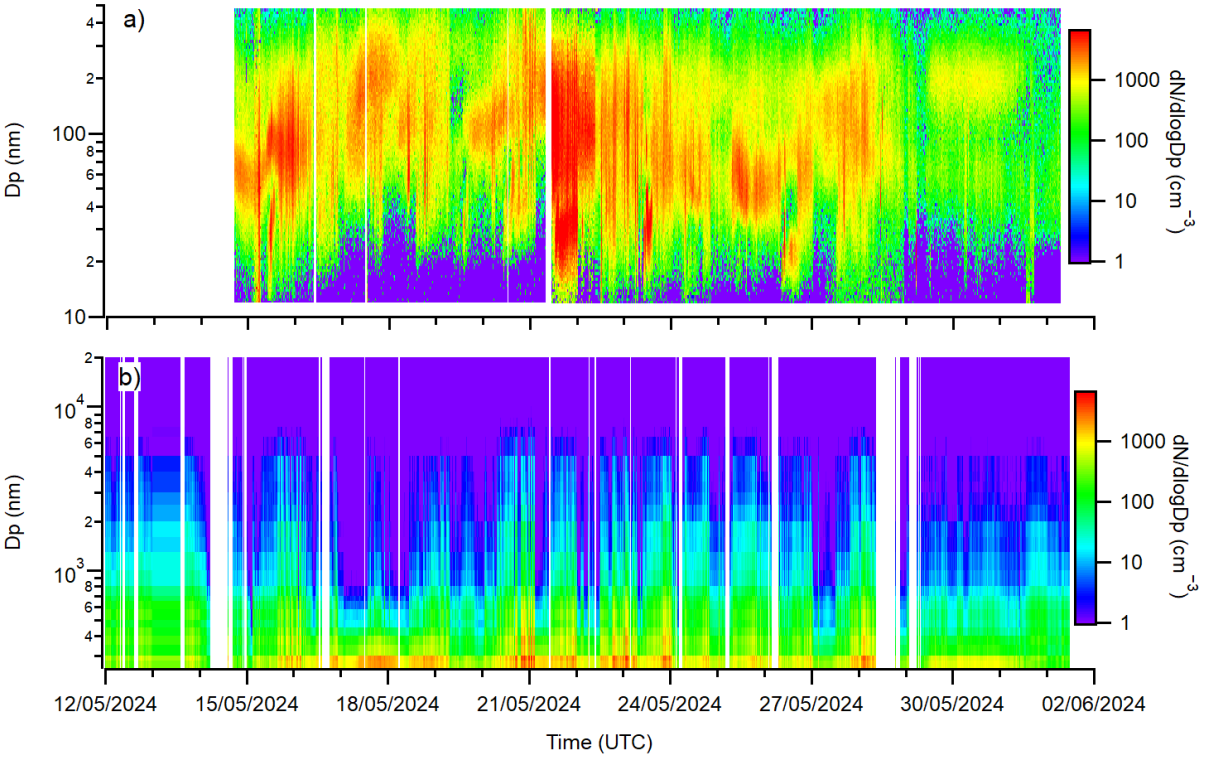


Figure S3. Temporal evolution of (a) surface wind speed and direction; (b) surface temperature and RH during the experiment.



30 **Figure S4. Time series of aerosol number size distributions measured by the (a) SMPS and (b) GRIMM during the campaign.**

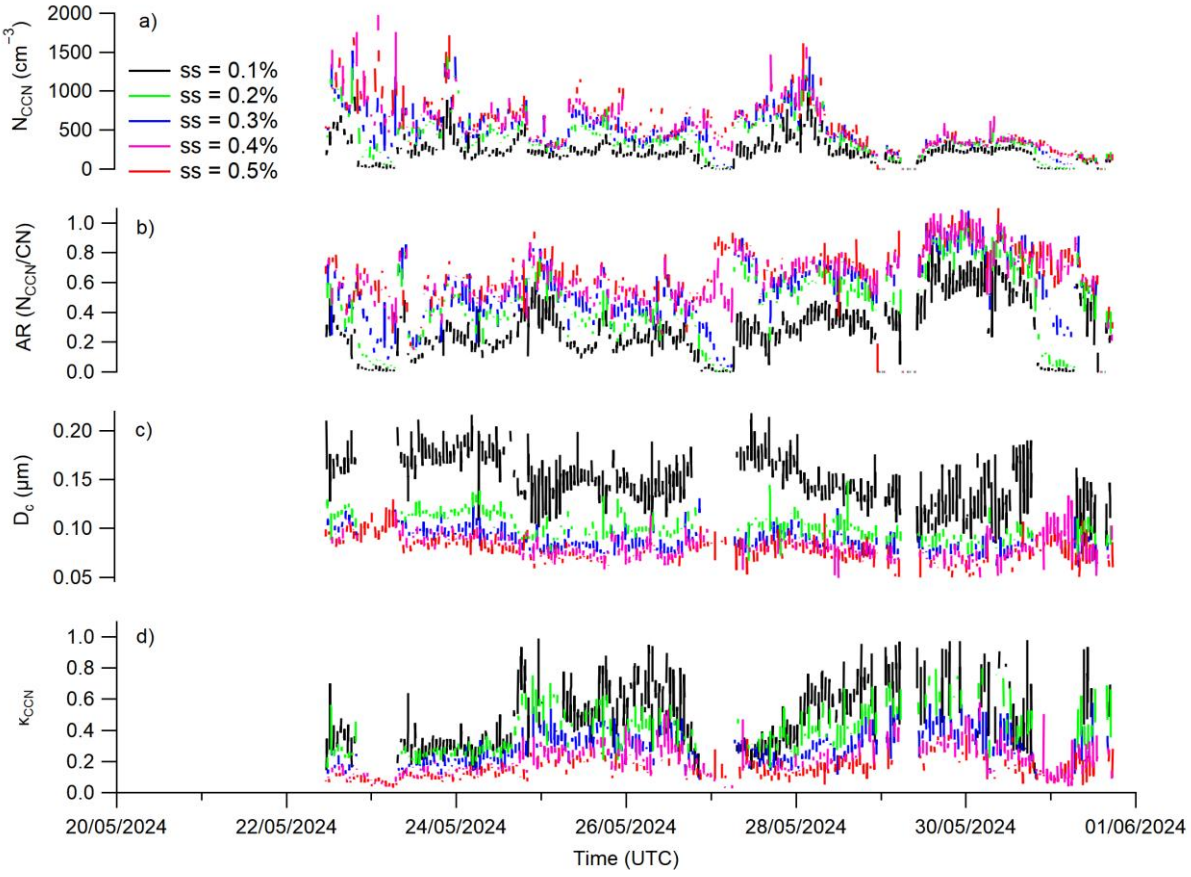


Figure S5. Time series of aerosol hygroscopic properties at different *SS* (0.1, 0.2, 0.3, 0.4, and 0.5%), including (a) N_{CCN}, (b) CCN activation ratio (AR= N_{CCN}/CN), where *CN* is the particle number concentration integrated from the SMPS size distributions, (c) activation diameter (D_c), and (d) CCN-derived hygroscopicity parameter (κ_{CCN}).

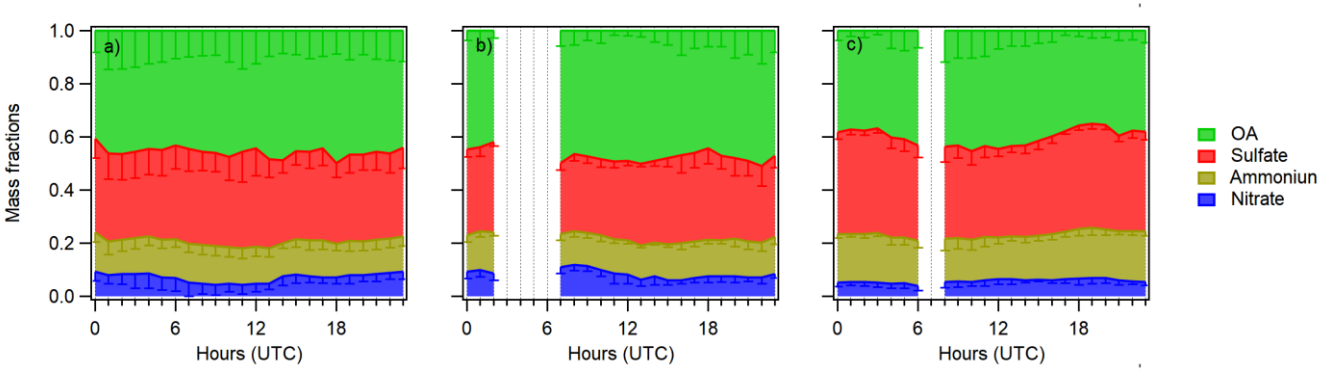


Figure S6. Diurnal profiles of average fractional contributions from ACSM chemical compositions for three periods. The bars represent the standard deviation.

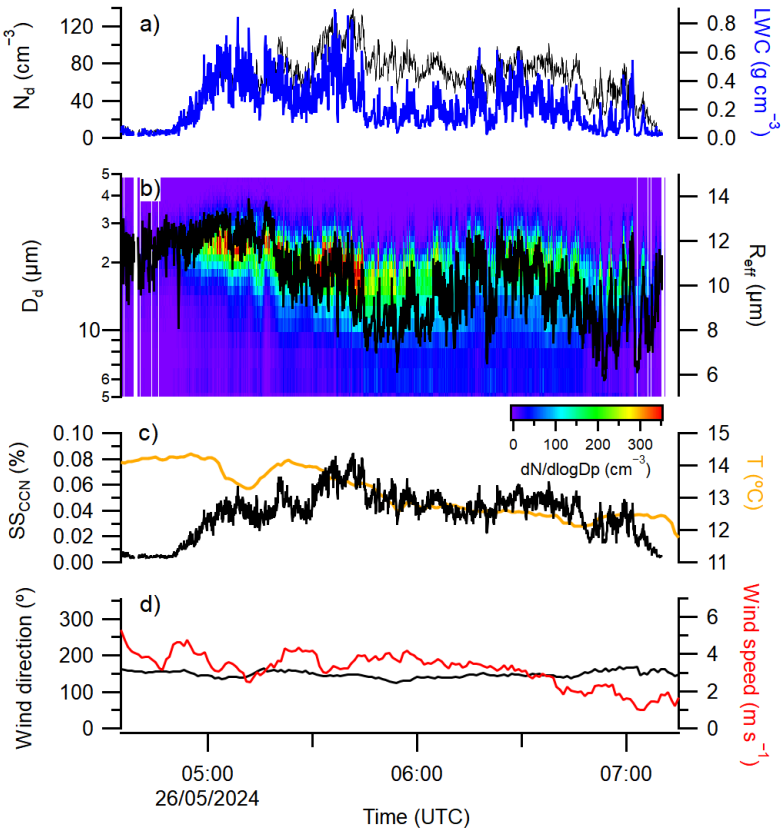


Figure S7. Example time series of fog properties and meteorological parameters in a locally formed fog event, including (a) droplet number concentration (N_d, left axis) and liquid water content (LWC, right axis), (b) droplet number size distribution (left axis) and effective radius (R_{eff}, right axis), (c) inferred SS_{CCN} (left axis) and temperature (T), (d) wind direction and speed.

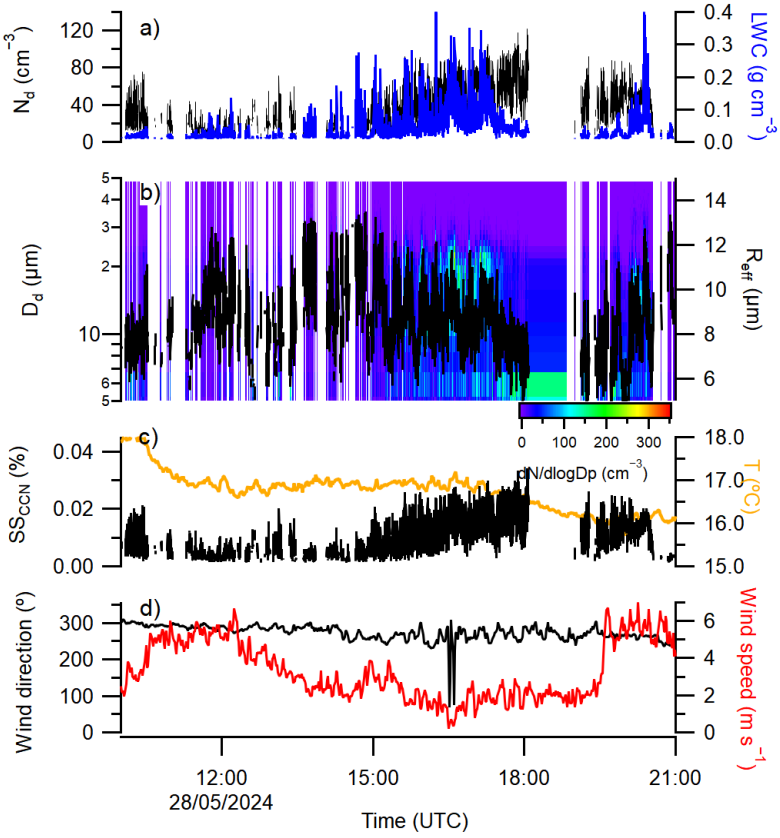


Figure S8. Example time series of fog properties and meteorological parameters in advection-driven fog event, including (a) droplet number concentration (N_d, left axis) and liquid water content (LWC, right axis), (b) droplet number size distribution (left axis) and effective radius (R_{eff}, right axis), (c) inferred SS_{CCN} (left axis) and temperature (T), (d) wind direction and speed.

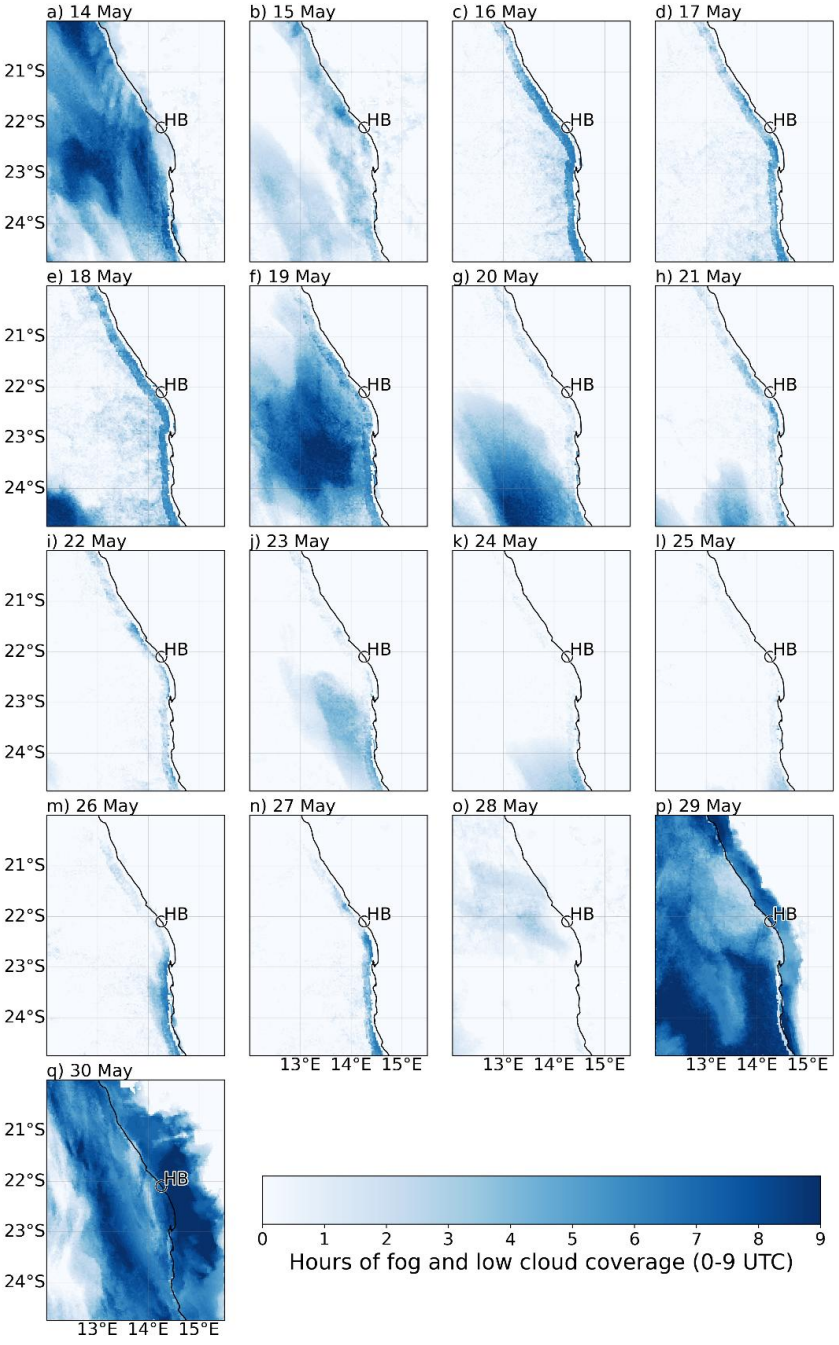


Figure S9. Daily occurrence duration of fog and low clouds between 00:00 and 09:00 UTC over the study region. The band of coastline-following clouds visible to a varying degree between May 16 and 27 is a satellite artifact of the CLAAS 3 data.

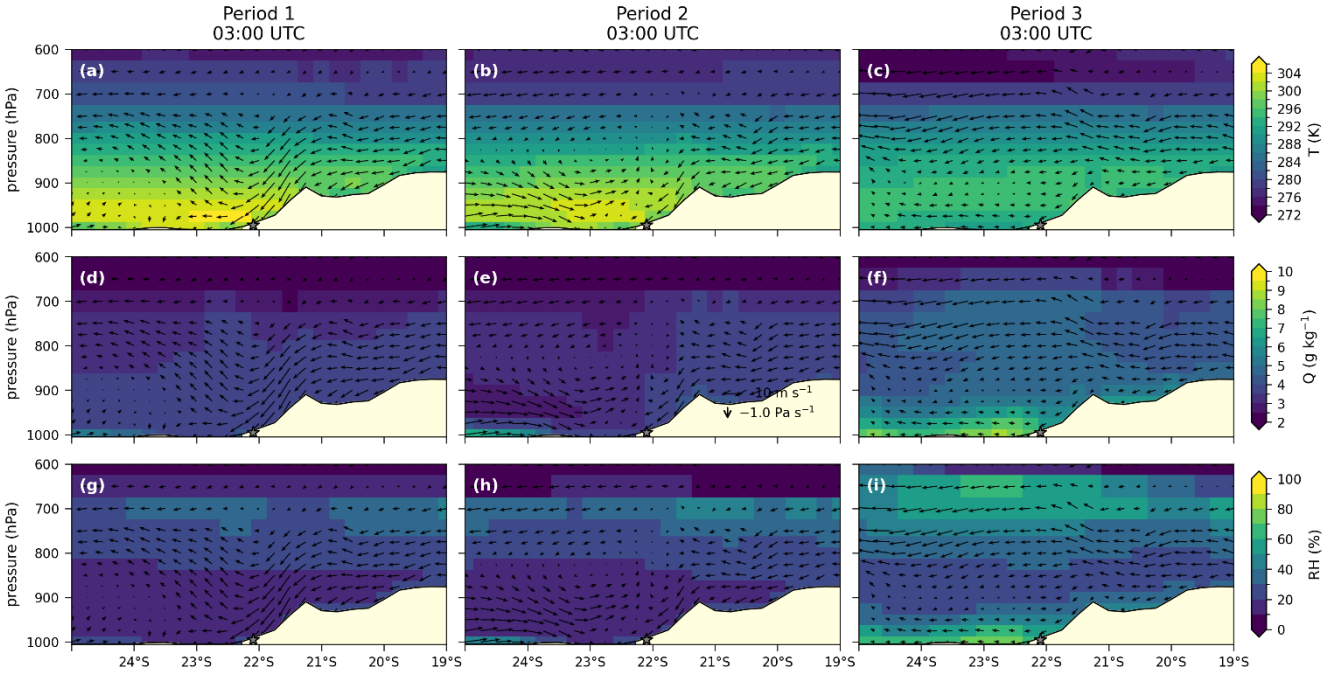


Figure S10. Regional atmospheric structure at Henties Bay (grey star) in longitude curtain plots at 14.26◦E, which was analyzed from ERA5. The columns represent mean vertical structure of the regional atmosphere at 3:00 UTC for the three identified periods. Shading shows temperature (T; a–c), specific humidity (q; d–f), and relative humidity (RH; g–i). Vectors represent the zonal wind component and vertical velocity (ω); negative ωdenotes upward motion. Reference vectors corresponding to 10 m $s^{-1}$and 1.0 Pa s^{-1} are shown in panel (e).

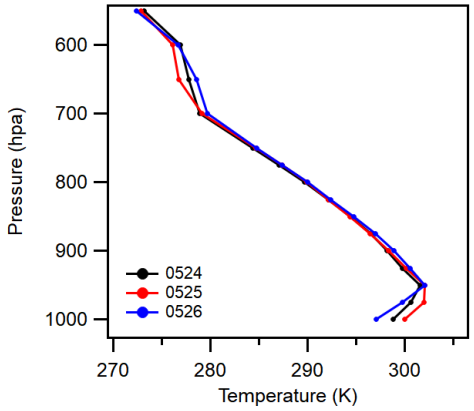


Figure S11. Daily vertical structure of temperature (K) at Henties Bay at 3:00 UTC.

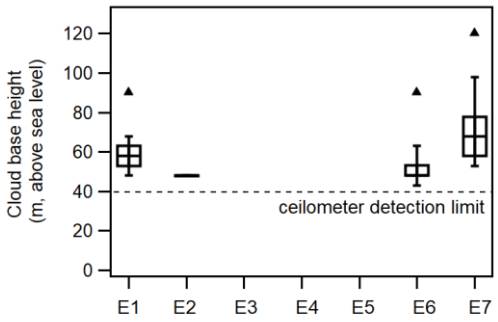


Figure S12. Cloud-base height distributions observed by the ceilometer at the coastal Swakopmund site during fog events E1-E7. Cloud-base heights are reported as meters above sea level. The dashed horizontal line indicates the ceilometer detection limit (~43 m above sea level). No fog or low-cloud base was detected at Swakopmund during E3-E5.

Reference

Alfarra, M. R., Paulsen, D., Gysel, M., Garforth, A. A., Dommen, J., Prévôt, A. S. H., Worsnop, D. R., Baltensperger, U., and Coe, H.: A mass spectrometric study of secondary organic aerosols formed from the photooxidation of anthropogenic and biogenic precursors in a reaction chamber, Atmos. Chem. Phys., 6, 5279–5293, https://doi.org/10.5194/acp-6-5279-2006, 2006.

Lambe, A. T., Onasch, T. B., Massoli, P., Croasdale, D. R., Wright, J. P., Ahern, A. T., Williams, L. R., Worsnop, D. R., Brune, W. H., and Davidovits, P.: Laboratory studies of the chemical composition and cloud condensation nuclei (CCN) activity of secondary organic aerosol (SOA) and oxidized primary organic aerosol (OPOA), Atmos. Chem. Phys., 11, 8913–8928, https://doi.org/10.5194/acp-11-8913-2011, 2011.

Liu, H. J., Zhao, C. S., Nekat, B., Ma, N., Wiedensohler, A., van Pinxteren, D., Spindler, G., Müller, K., and Herrmann, H.: Aerosol hygroscopicity derived from size-segregated chemical composition and its parameterization in the North China Plain, Atmos. Chem. Phys., 14, 2525–2539, https://doi.org/10.5194/acp-14-2525-2014, 2014.

Silvergren, S., Wideqvist, U., Ström, J., Sjogren, S., and Svenningsson, B.: Hygroscopic growth and cloud forming potential of Arctic aerosol based on observed chemical and physical characteristics (a 1 year study 2007–2008), J. Geophys. Res., 119, 14080–14097, https://doi.org/10.1002/2014JD021657, 2014.

Topping, D. O., McFiggans, G. B., and Coe, H.: A curved multi-component aerosol hygroscopicity model framework: Part 1 – Inorganic compounds, Atmos. Chem. Phys., 5, 1205–1222, https://doi.org/10.5194/acp-5-1205-2005, 2005.